JOURNAL OF COMPUTATIONAL PHYSICS **88**, 114–130 (1990)

NUT: A Fast 3-Dimensional Neutral Transport Code

P. M. VALANJU

Fusion Research Center, Department of Physics,
The University of Texas at Austin, Austin, Texas 78712

Received December 20, 1988; revised May 16, 1989

We present a fast code for calculating the steady-state transport of neutral atoms in an axially symmetric background plasma. The primary source for the neutrals is not required to have any symmetry. Due to the small momentum transfer involved in charge exchange collisions, the secondary neutral atoms emerge with the local velocity distribution of the plasma ions. Some neutrals are lost due to ionization. The neutral transport is described by an integral equation for the neutral source. With a careful choice of a three-dimensional spatial grid, the small scale features of these equations can be integrated analytically to yield a set of algebraic equations that can be solved by only a few iterations. This results in a fast and compact algorithm which can be used as a subroutine in plasma simulation codes. Comparisons with other currently used codes and with experimental measurements show good agreement. © 1990 Academic Press, Inc.

1. INTRODUCTION

In order to describe plasma transport processes, it is important to know the neutral density accurately throughout the plasma. The neutral atoms enter the plasma at the edge with small energies (typically a few electron volts). However, since charge exchange and ionization cross sections are comparable, a significant fraction of the cold neutrals gets replaced by hot ones which can penetrate the plasma much further. Due to their long mean free paths at high energies, even a small number of such neutrals reaching the hot central plasma can charge exchange and convect energy straight to the wall. In medium-size tokamaks this convective loss can be significant. To make meaningful comparisons of various transport theories with experiment, it is important to measure and calculate the neutral transport. For the outer regions of the plasma the radial, poloidal, and toroidal dependence of the neutral source can be measured using spectroscopic techniques. However, a direct measurement of the neutral source deep in the plasma is a very difficult experiment. Diagnostic neutral beam experiments can potentially yield some information, but to interpret them it is essential to know the relative contributions to the signals coming from the primary and the secondary (halo) neutrals.

The neutral transport problem is similar to neutron transport. The earlier work was mainly analytic in which existing solutions for neutron transport were adopted and extended [1–4]. However, for plasmas with arbitrary density and temperature

0021-9991/90 $3.00

profiles, one has to use numerical techniques. The first such codes developed [5–11] were mainly non-stochastic, one-dimensional codes to be used in one-dimensional plasma transport calculations. The development of two-dimensional and three-dimensional plasma transport codes along with the desire to include more physical processes motivated the use of Monte-Carlo techniques [12–16]. The existing neutral transport codes have been nicely summarized by Tendler and Heifetz [17] (many of them have been published in *J. Comput. Physics*). They also give a table of various modeling problems and the necessory geometries, from which it can be seen how the choice of a neutral code is dictated by the type of transport simulation. The Monte-Carlo codes such as DEGAS [13] make almost no simplifying assumptions and are therefore expensive to run. At the other end are the fast codes such as ANTIC [9] or SPUDNUT [7], which assume some symmetry (cylindrical or slab) for the source and the plasma. Between these two alternatives is an area where one can sacrifice some detail in the physical processes while retaining the higher dimensionality. Since the actual neutral source in most machines does vary both poloidally and toroidally (although the plasma is often toroidally symmetric), there is considerable incentive for developing a code that lies somewhere in between and can be used by plasma simulation codes as a subroutine.

The code NUT (neutral transport) described here tries to fit in this region. It is accurate, compact, and fast enough to be used in three-dimensional simulations of axially symmetric plasmas (with any cross section) with an arbitrary external source of neutrals (such as an uneven source from the walls, or a diagnostic neutral beam, or a divertor). The compactness and the speed are achieved by observing that in many problems of interest the plasma parameters (such as the ion density and temperature) vary only slowly over lengths of the order of the mean free paths of the neutrals. Hence, by carefully identifying the smallest relevant scale length in the problem and analytically integrating out all smaller scale features, one can keep the number of grid points small and still get accurate answers.

The next section describes the basic integral equation used in the problem and the corresponding assumptions. In Section 3, we show how a proper choice of spatial grid points along with a carefully chosen averaging process turns the integral equation into a small set of algebraic equations which can be solved quickly in a few iterations. Finally, in Section 4, we compare our results with other codes and with experiments.

2. THE BASIC EQUATION AND THE ASSUMPTIONS

We start with a given plasma column whose density and temperature are independent of the toroidal position (z). The plasma can have any arbitrary cross section. Neutrals injected into the plasma from various external sources are either lost due to ionization (from electron or ion impact) or change their energy and momentum due to a charge exchange process. We denote by the source $\phi(\mathbf{r}, E)$ the total number of neutrals produced per unit volume per second at the point $\mathbf{r}$ with energy E. This source consists of the externally introduced primary wall and beam neutrals $\phi^0(\mathbf{r}, E)$, and the hot secondaries created at $\mathbf{r}$ by neutrals coming from all other points

$$\phi(\mathbf{r}, E) = \phi^0(\mathbf{r}, E) + \int d^3r'\, dE'\, G(\mathbf{r}, \mathbf{r}'; E, E')\, \phi(\mathbf{r}', E'), \tag{1}$$

where $G(\mathbf{r}, \mathbf{r}'; E, E')$ is the probability that a neutral born at $\mathbf{r}'$ with energy E' will go unaffected to $\mathbf{r}$ and charge exchange into a neutral of energy E. For a given external source ϕ^0, the solution of the linear equation (1) represents the net source ϕ, from which all other quantities of interest can be calculated directly.

Like all other codes mentioned in this paper, our calculation of the neutral source is perturbative, i.e., the effect of the neutrals on the plasma is not calculated. Hence the propagator $G(\mathbf{r}, \mathbf{r}'; E, E')$ is independent of the source ϕ, and shares all the symmetries of the background plasma. In particular, it is invariant under translations along the plasma axis (the z axis). The forms of G are different depending on whether the beginning and the end points are on the wall or in plasma. However, both forms contain the geometrical attenuation factor in going from $\mathbf{r}$ to $\mathbf{r}'$:

$$G_0(\mathbf{r}, \mathbf{r}', E) = \frac{\exp(-\tau(\mathbf{r}, \mathbf{r}', E))}{4\pi\, |\mathbf{r} - \mathbf{r}'|^2}, \tag{2}$$

where

$$\tau(\mathbf{r}, \mathbf{r}', E) = \int_{\mathbf{r}}^{\mathbf{r}'} a^{\text{tot}}(\mathbf{r}'', E)\, d\mathbf{r}'', \tag{3}$$

and $a^{\text{tot}}(\mathbf{r}'', E)$ is the total inverse mean free path of a neutral with energy E at the point $\mathbf{r}''$. This total includes all possible processes that can knock the neutral out of its original path, viz., charge exchange or ionization by ion or electron impact. The charge exchange and ionization cross sections used by NUT are identical to those used in ANTIC.

To convert G_0 into the full propagator, we have to multiply it by the initial and final neutral distributions. For neutrals born in the plasma in a charge exchange process, the momentum transfer is small. Hence the outgoing neutral has the energy distribution of the target ions only, while the incoming neutral energy decides the cross section for the charge exchange process. We assume that the ions have an isotropic Maxwellian distribution at the local temperature. The neutrals coming from the wall are assumed to have a cosine distribution in angle (corresponding to a diffuse source), and an energy distribution given by the reflection function $R(E, E')$, which is the probability that a neutral with energy E will be reflected from the wall with energy E'. Instead of the energy independent reflection coefficient used in ANTIC, we have used a more realistic reflection coefficient given by McCracken and Stott [18]. Since the average energy of the reflected particle is given as a function of (and is smaller than) the incident energy, $R(E, E')$ is a vector rather than a matrix. Depending on the location of the initial and final points, we get four possible forms for G:

$$G_{pp} = M(\mathbf{r}, E)\, a^{cx}(\mathbf{r}, E')\, G_0(\mathbf{r}, \mathbf{r}'), \tag{4}$$

$$G_{pw} = M(\mathbf{r}, E)\, a^{cx}(\mathbf{r}, E')\, G_0(\mathbf{r}, \mathbf{r}') \cos(\theta(\mathbf{r}, \mathbf{r}')), \tag{5}$$

$$G_{wp} = R(E, E') \cos(\theta(\mathbf{r}, \mathbf{r}'))\, G_0(\mathbf{r}, \mathbf{r}'), \tag{6}$$

$$G_{ww} = R(E, E') \cos(\theta(\mathbf{r}, \mathbf{r}'))\, G_0(\mathbf{r}, \mathbf{r}') \cos(\theta(\mathbf{r}, \mathbf{r}')), \tag{7}$$

where G_{ab} denotes the propagator going from b to a, the subscripts p and w stand for the plasma and the wall, $a^{cx}(\mathbf{r}, E')$ is the charge exchange inverse mean free path for a neutral of energy E at the point $\mathbf{r}$, $\theta(\mathbf{r}, \mathbf{r}')$ is the angle between the ray joining the points $\mathbf{r}$ and $\mathbf{r}'$ and the normal to the wall at the proper end of the ray, and $M(\mathbf{r}, E)$ is the Maxwellian with the ion temperature at the point $\mathbf{r}$.

The external source $\phi^0(\mathbf{r}, E)$ comes either from the wall, which provides a diffuse source of cold, low energy neutrals (0.1 to 20 eV), or from other sources such as the high energy diagnostic neutral beam which creates first generation neutrals via charge exchange with plasma ions. For more complex configurations, any arbitrary external sources can be introduced on the wall or in the plasma.

Symbolically, Eq. (1) can be written as

$$\phi = \phi^0 + G\phi. \tag{8}$$

Due to the exponential attenuation factor in G, the norm of $G\phi$ (defined in some averaged sense) is smaller than the norm of ϕ, allowing us to use iteration to solve Eq. (1) with ϕ^0 as the initial guess

$$\phi = \phi^0 + G\phi^0 + GG\phi^0 + GGG\phi^0 + \cdots. \tag{9}$$

Each iteration corresponds to a new generation of neutrals, i.e., at the nth step, we get the effects of n successive scatterings of a neutral either in plasma or on the wall. This is completely equivalent to using a linear equation solver which inverts the matrix $[1 - G]$. Since the ionization and charge exchange cross sections are comparable, the iteration converges reasonably fast. For a small matrix G (with small number of grid points, as in ANTIC) iteration is slower than the linear equation solver. However, when the number of grid points is large, the iterative technique works much faster.

Since the forms of G depend on whether the two points are on the wall or in the plasma, we separate Eq. (8) into

$$\phi_p = \phi_p^0 + G_{pp}\phi_p + G_{pw}\phi_w, \tag{10}$$

$$\phi_w = \phi_w^0 + G_{wp}\phi_p + G_{ww}\phi_w. \tag{11}$$

We can formally eliminate the wall source ϕ_w by solving the second equation, and substituting the result into the first one to obtain

$$\phi_w = \phi_p^0 + G_{pw}(1 - G_{ww})^{-1}\,\phi_w^0 + (G_{pp} + G_{pw}(1 - G_{ww})^{-1}\,G_{wp})\,\phi_p. \qquad (12)$$

Note that this equation is almost the same as in ANTIC, except for the $(1 - G_{ww})^{-1}$ factor in front of the external wall source ϕ_w^0. This factor would make no difference if the reflection coefficient at the wall were set to zero. However, for non-zero reflection coefficient, ANTIC is expected to give a slightly larger penetration than the correct answer.

3. THE METHOD OF COMPUTATION

In order to numerically solve Eq. (1) we choose spatial and energy grids, and write it in a discretized form as

$$\phi(i) = \phi^0(i) + \sum_j G(i, j)\,\phi(j), \qquad (13)$$

where the index i is used to collectively denote the position and energy bin over which the continuous quantity is averaged. The sum in this equation extends over both the plasma and the wall points. Since the energy dependence of the source ϕ in the plasma is always given by the normalized local Maxwellian function $M(\mathbf{r}, E)$, we can factor it out to define a reduced source ψ in the plasma

$$\phi(\mathbf{r}, E) = \psi(\mathbf{r})\,M(\mathbf{r}, E). \qquad (14)$$

Using this in Eqs. (10) and (11), we get

$$\psi(i) = \psi^0(i) + \sum_{\text{plasma}} G_{pp}(i, j)\,\psi_p(j) + \frac{1}{M(i, E)} \sum_{\text{wall}} G_{pw}(i, j, E')\,\phi_w(j, E'), \qquad (15)$$

for points in the plasma, and

$$\phi_w(i, E) = \phi_w^0(i, E) + \sum_{\text{plasma}} G_{wp}(i, j)\,\psi_p(j) + \sum_{\text{wall}} G_{ww}(i, j; E, E')\,\phi_w(j, E'). \qquad (16)$$

for points on the wall. All energy dependence disappears from the sum over plasma points, which now runs over only the three-dimensional spatial volume of the plasma. The wall point sum still runs over the two-dimensional wall surface and the one-dimensional energy grid. The Green's functions used in these equations are the discretized forms of the ones in Eq. (4)–(7). The indices i and j denote the positions of the target and the source grid points. The exact procedure to go from the continuum forms (4)–(7) to these discretized forms will be spelled out in the remaining part of this section.

Numerical calculation of the three-dimensional sum in Eq. (15) requires a lot of care because of the singularity in G at short distances. Of course, the integral is convergent, but its discretized form can be subject to problems unless this divergence is explicitly cancelled by the volume element. This can only be done if the integral is performed over the relative co-ordinate $\mathbf{s} = \mathbf{r} - \mathbf{r}'$. Each source point can now be denoted either by its absolute location $\mathbf{r}'$, or by its location relative to the target point $\mathbf{r}$, viz., by $(\mathbf{r}, s, \omega)$, where $\mathbf{r}$ is the target point, ω labels the direction of the ray from the source to the target point, and s is the distance between the two points along the ray. To avoid confusion, we shall use $\chi(\mathbf{r}, s, \omega)$ instead of ϕ to denote the source at $\mathbf{r}'$ written in the relative co-ordinates. The three-dimensional integrals over source points $\mathbf{r}'$ for each target point $\mathbf{r}$ can in general be written as

$$I(\mathbf{r}) = \int s^2\, ds\, d\omega \frac{\exp(-\int ds'\, a^{\text{tot}}(s, s'))}{4\pi s^2} \chi(\mathbf{r}, s, \omega), \tag{17}$$

in which the troublesome factor s^2 cancels. We first carry out the integration over s along a ray starting from the target point, and then average the answer over many rays. Over each ray, the s integral has the form

$$I(\mathbf{r}, \omega) = \int_0^\infty ds \exp\left(-\int_0^s ds'\, a^{\text{tot}}(s, s')\right) \chi(\mathbf{r}, s, \omega). \tag{18}$$

To be able to do this without extra interpolations, at avery target point the source points must lie on rays starting from the target. This forces us to choose a spatial grid which looks identical from every target point, i.e., a lattice. A convenient choice is the cubic lattice. At each point, we have 26 rays going to the 6 faces, 12 edges, and 8 vertices of the cube surrounding that point. These give us ample angular resolution. In addition, since each bin in the lattice has the same volume over which the source is averaged, we can use the lattice spacing δ as our unit of length. This saves us many multiplications and divisions by δ in the program.

To achieve high calculational speed we must decrease the total number of points needed, i.e., choose as large a δ as possible. To do this, we note that there are two distinct length scales in the problem. The propagators die off over length scales of the order of the mean free paths (varying from 0.01 to 100 cm depending on the energy), but the mean free paths themselves change very slowly over length scales comparable to the plasma size (about 5 cm). We can use the larger length scale for the grid spacing if we manage to analytically do the integrals over one grid size. This is in fact possible. To see this, consider the typical integral in Eq. (18). If we label the points on the ray by an index i starting with 0 for the target, the integral becomes

$$I(\mathbf{r}, \omega) = \sum_{i=0}^{I-1} I_i(\mathbf{r}, \omega), \tag{19}$$

where l is last point on the ray and $I_i(\omega)$ is the integral between the ray points i and $i+1$. Each of these integrals between two successive points on the ray can be done analytically if we approximate the slowly varying quantities such as the source ϕ and the inverse mean free path a^{tot} by polynomials over this interval. In fact, a first order expansion is quite adequate, though for greater accuracy the expansions can be carried to higher orders. All the pieces $I_i(\mathbf{r}, \omega)$ are then summed up in Eq. (19) to give the integrals $I(\mathbf{r}, \omega)$ along each ray, which are finally averaged over the 26 directions. In the resulting expression the sources $\phi(j)$ appear linearly, multiplied by functions of plasma parameters which are just the discretized propagators $G_{pp}(i, j)$ of Eq. (15). Since these propagators are indepedent of the source, they need to be calculated only once before the iteration begins.

This scheme is also well suited for calculating the wall-to-plasma, plasma-to-wall, and wall-to-wall propagators, which involve two-dimensional integrals over the wall surface. For each plasma point, we find the nearest point on the wall, calculate the integrals over four (or eight) rays starting from that point, and then add them up. The integral over each ray is broken up into pieces going from one wall point to next. Within each piece, the mean free paths and the sources are expanded in polynomials and the integral is done analytically. This is possible for any given local curvature of the wall (in each direction). Again, the resulting expressions are linear in sources, and so the discretized propagators can be identified. This is important, since otherwise we cannot write the equations in the form (15)–(16). The summations at all the target points in these equations can be vectorized, or done paralally, resulting in a very high speed.

Details of all the propagator calculations are given in Appendix A. We have tested this scheme to calculate some exactly solvable integrals in which the grid size varied between 0.1 to 10 times the mean free path, and the answer was accurate to within a few percent. Since the time and memory requirements increase as the sixth power of the inverse grid size, without this fast integration scheme this code could not have met the demands of high speed and small memory.

A further small increase in speed results from restricting the integration volume to include only the source points that lie within a few mean free paths of the target. This reduces one of the dimensions of the $G(i, j)$ matrix and speeds up the iterations without noticeable loss of accuracy. In addition, one could use extra symmetrics (such as top-bottom, or cylindrical) of the plasma (not of the source) to speed up the propagator calculations. However, this does not reduce the main time consuming part—the iteration time. It also adds extra code and makes the program less general. In any case, when used in a time-stepping plasma simulation code, the propagators need to be recalculated only when the plasma changes substantially, which is not at every time step. For these reasons, we have not added any symmetry restrictions on our code.

In order to run the code, a suitable grid constant is chosen, and the plasma is fitted in a three dimensional box. The plasma and the wall shape are specified. Since the wall-to-plasma propagators are treated separately, the wall points need not lie on the cubic grid. They are chosen on the wall surface to give adequate resolution.

For example, for the TEXT [19] tokamak with a wall minor radius of 30 cm, the choice of a grid constant of 5 cm and a grid of 32 equally spaced poloidal and 5 [redacted] since all the geometry need not be recalculated every time the code is run. Given the plasma profiles and the external sources, this subroutine calculates the neutral source $\phi(\mathbf{r})$ at all points in the plasma and on the wall. From this, the various quantities of interest such as the neutral density, the rate of change of plasma particle and energy densities, the average energy of neutrals, and the neutral flux at the wall are easily calculated.

4. NUMERICAL RESULTS AND COMPARISON WITH EXPERIMENT

As a first step, we compared the results of our code (NUT) with ANTIC (which in turn has been compared with other codes in Ref. [9]) for the cylindrically symmetric case with zero reflection coefficient over a wide range of plasma parameters and sizes. For the comparison, the Maxwellian was collapsed to a delta function at $3/2T$. Energies of the cold neutrals coming from the wall were set to the same nominal values of 2 and 20 eV in both codes. The fluxes at the two energies were set equal. Since both NUT and ANTIC are linear in the source, the wall sources have to be given from outside, i.e., these codes themselves do not contain any physics that specifies the input neutral flux at the wall. After setting everything identical in the two codes, we get good agreement for all the cases we have tried. Some of the comparisons for different central plasma densities are shown in Fig. 1. For a tokamak like TEXT with a 30 cm minor radius, a grid constant of 5 cm is quite adequate. Approximately 10 iterations are needed to get good convergence.

In the wall-to-plasma terms G_{pw} and G_{wp}, it is important to use the correct wall curvature whenever it is comparable to the mean free path of the high energy neutrals. A flat wall does not give a good answer, nor does a slab plasma. In particular, the neutral source deep in the plasma comes out too small if a flat wall is used. In TEXT, this neutral penetration is significant because the neutral mean free paths are comparable to the plasma size for the high energy atoms. However, for larger tokamaks with less neutral penetration, the error may not be so crucial. In all cases, the direct wall-to-wall term is not significant due to the $\cos^2(\theta)$ factor. This factor is very small unless the starting and the final wall sections almost face each other, but then the distance between them is large. Only in geometries with regions of very sharp wall curvatures (such as a divertor chamber) will this factor be important. Otherwise we can safely turn it off to save computational time.

Next we compare our results with experimental measurements for the cylindrical TEXT plasma with a more realistic non-uniform wall source which has been measured by Rowan *et al.* [20] using spectroscopic observations of H_α emission.

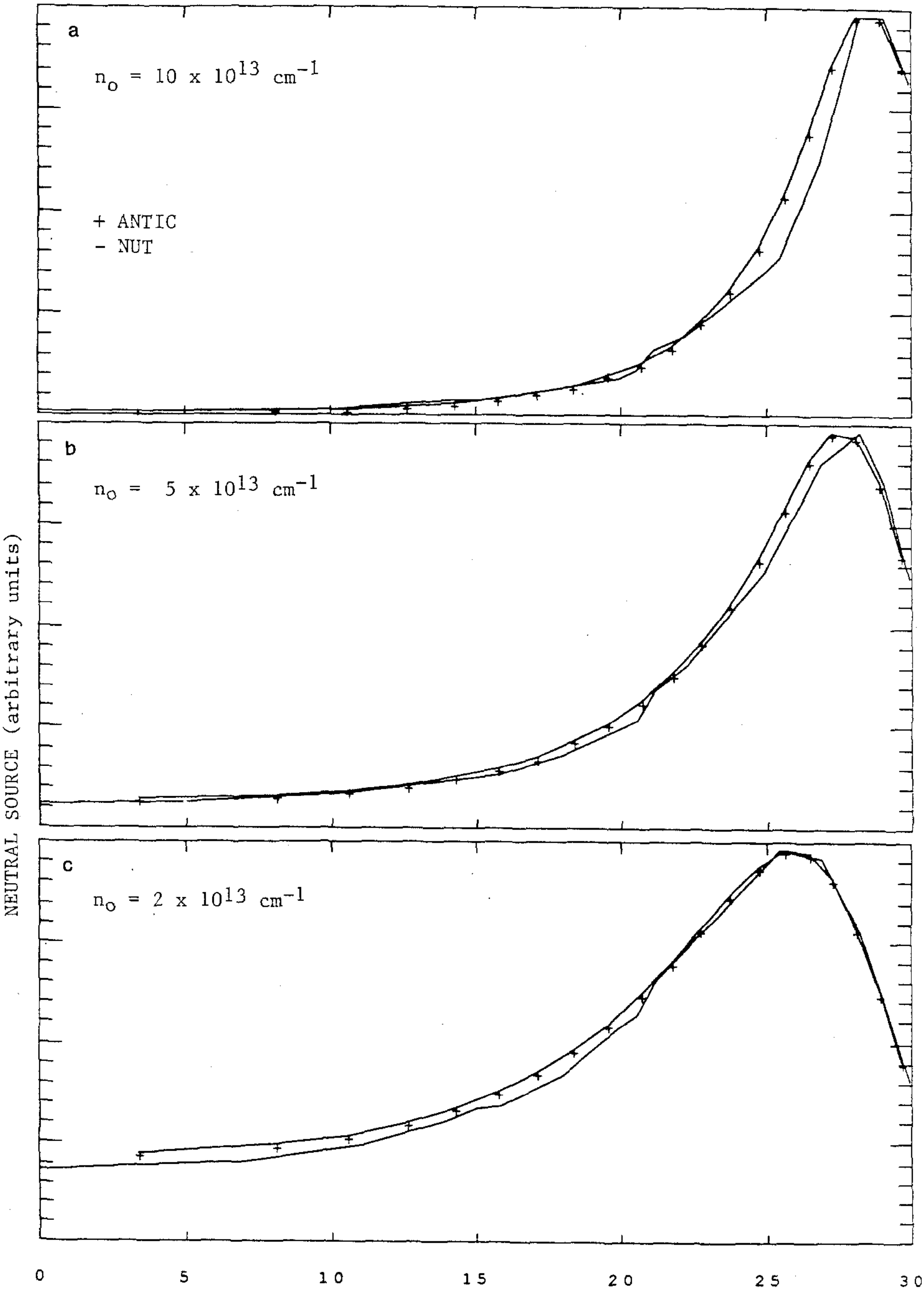

FIG. 1. Comparison of NUT calculations with ANTIC. The neutral source ϕ is plotted as a function of minor radius (cm). Since the equations for ϕ are linear, we arbitrarily normalize all sources to 1. All parametes are set the same for both codes. The Hydrogen plasma parameters are $n_e = n_i = (n_0 - n_w)[1-(r/a)^2] + n_w$, $T_e = (T_{e0} - T_{ew})[1-(r/a)^2]^2 + T_{ew}$, and $T_i = (T_{i0} - T_{iw})[1-(r/a)^2]^2 + T_{iw}$. The plasma radius a is 30 cm. The temperatures are held fixed with $T_{e0} = T_{i0} = 1000$ eV. All wall values are one-tenth of the central values. The neutral wall source is constant at all wall points. The two cold neutral energies are 2 and 20 eV. The wall reflection coefficients are set to zero.

The experiment consists of three distinct parts. The chord averaged values of H_α radiation at various minor radii in one toroidal plane far from the limiter is measured using a rotating mirror arrangement. After Abel inversion, this yields the dependence of the source on minor radius. The net source integrated along the major radius in the equatorial plane is measured by light monitors at eight different toroidal locations while the source at the limiter is monitored by a TV camera. The toroidal dependence of this integrated source is an exponential with a sharp maximum at the limiter. It is found that these integrated measurements are consistent with a source of the form

$$S(\mathbf{r}, \theta, z) = S_0(r)(1 + \beta \cos(\theta))[S_L \exp(-z/z_0) + S_w], \tag{20}$$

where z is the toroidal distance from the limiter, θ is the poloidal angle, S_L and S_w are the magnitudes of the measured source at the limiter and the wall, and the radial dependence $S_0(r)$ has been normalized to a maximum of one (see Figs. 1–4 of Ref. [20]). The toroidal fall-off length z_0 varies from 7 to 5 cm as the density varies from 2×10^{13} to 6×10^{13}/cc. The ratio of the limiter to wall source varies between 40 and 100 for these densities. The poloidal asymmetry factor β varies between 0.8 and -0.5 depending on the plasma position. By integrating the above form over the toroidal direction, it can be seen that with a major radius of 1 m, a value of $z_0 = 6$ cm implies that about half the net source in TEXT comes from the limiter and the other half from the wall.

Since linear codes such as NUT require the specification of an external source, to simulate these conditions we assume a non-uniform external wall source which is bigger at the limiter (at $z = 0$) than at the wall and which is concentrated at the outer part of the wall (near $\theta = 0$). The physics of why the external source has this asymmetry is outside the scope of all these codes. The structure of the calculated source in one poloidal plane (the $r - \theta$, or equivalently the $x - y$ plane) is shown in Fig. 2, while its dependence on r and z is shown in Fig. 3. As can be seen from Fig. 2b, the poloidal $\cos(\theta)$ dependence can be reproduced by concentrating the source at the outer edge. Since the dependence of the external source on plasma position is unknown, we can only see qualitative agreement in this direction, *viz*, whenever the plasma rides on the outer edge of the limiter, the source is peaked on the outside. However, in the toroidal direction we do not have much freedom. If we use a large source at the limiter ($z = 0$) and a small uniform source at the wall, we get the exponentially peaked source seen in Fig. 3b. We integrate this source along the major radius at different z values and calculate its decay length, which is plotted in Fig. 4 along with the experimental measurements at many different densities. The agreement of the absolute value as well as the variation with density of z_0 with experimentally measured values is good. We also note that z_0 essentially measures the toroidal fall-off length and is independent of the ratio of S_L to S_W. This agreement gives us confidence in the absolute values of the mean free paths, their variation with density, the wall deposition model we have used, and our algorithm.

Part of this agreement may depends on the values (2 and 20 eV) used for the

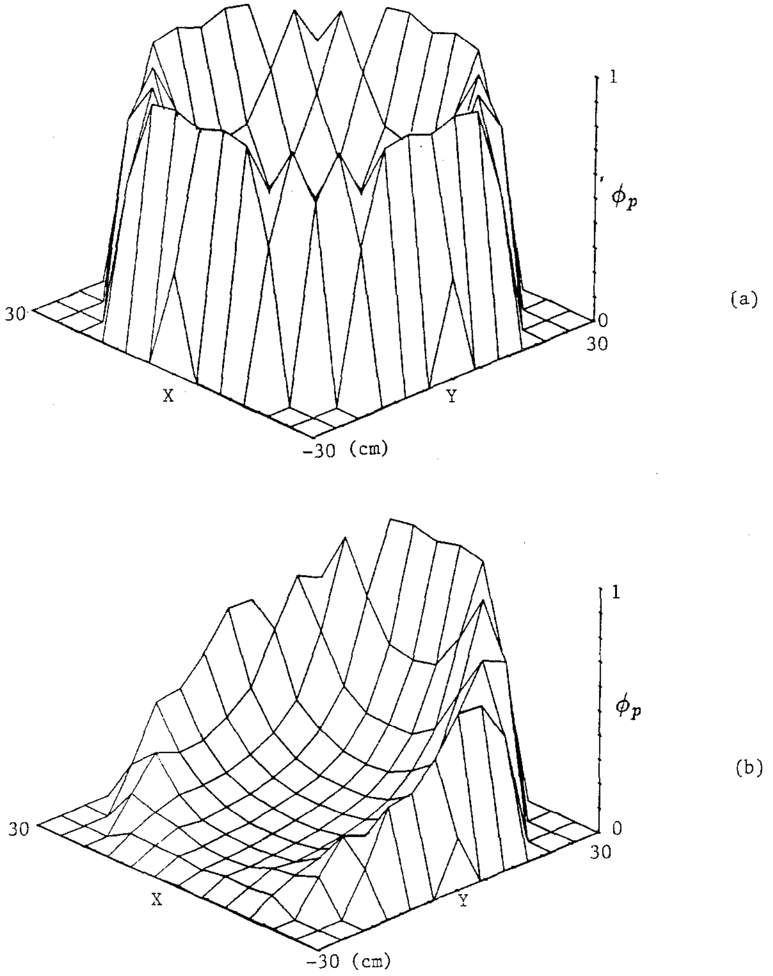

FIG. 2. The neutral source in the $z = 0$ plane calculated by NUT for the same plasma conditions as in Fig. 1b. In Fig. 2a the wall source is constant, while in Fig. 2b it has a $\cos(\theta)$ dependence.

energies of the incoming cold neutrals from the wall. In a Franck–Condon dissociation of a molecule, we expect one of the atoms to carry small (less than a few electron volts) and the other a large (5 to 20 eV) energy. Since the physics of these processes is outside the scope of NUT and the energies and the fluxes of neutrals from the wall are an external input, we have tried various combinations within the above limits. We always set the two fluxes equal. The decay length z_0 seems to be governed more by the higher generations than by direct deposition from the wall, and hence the value of z_0 is not very sensitive to the wall-neutral energies.

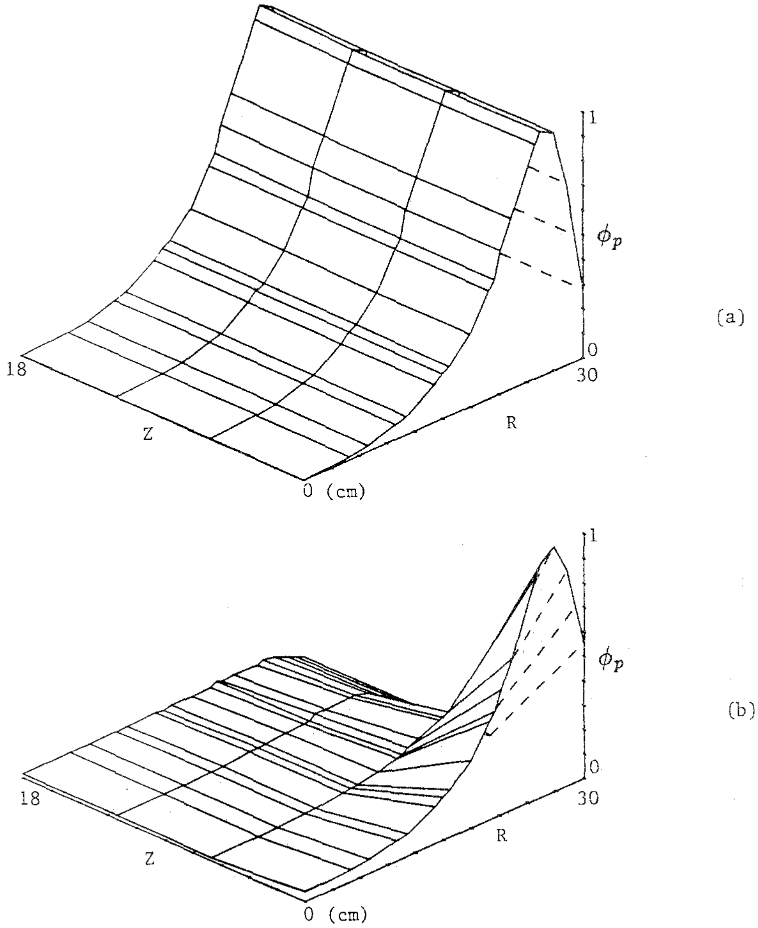

FIG. 3. The r and z dependence of the neutral source calculated by NUT for the same plasma conditions as in Fig. 1b. The wall source is constant in Fig. 3a, while in Fig. 3b it is set to 50 at all points on the limiter ($z=0$) and to 1 at all points on the wall ($z>0$), which are the values suggested in Ref. [20] for the TEXT plasma.

The measurements of the radial dependence of the source are Abel inverted from chord averaged measurements in which the small source near the center gets masked by the large value near the edge. The measurement is thus good only for the outer region of the plasma, where our calculations fit very well with the experiment. The small central source, however, is important in plasma transport calculations since it can lead to a large convective loss term from these neutrals charge exchanging with plasma ions. Given the agreement with the rest of the data, we feel confident about the predicted value of the source for the inner part of the plasma. A direct measurement of it would be very useful.

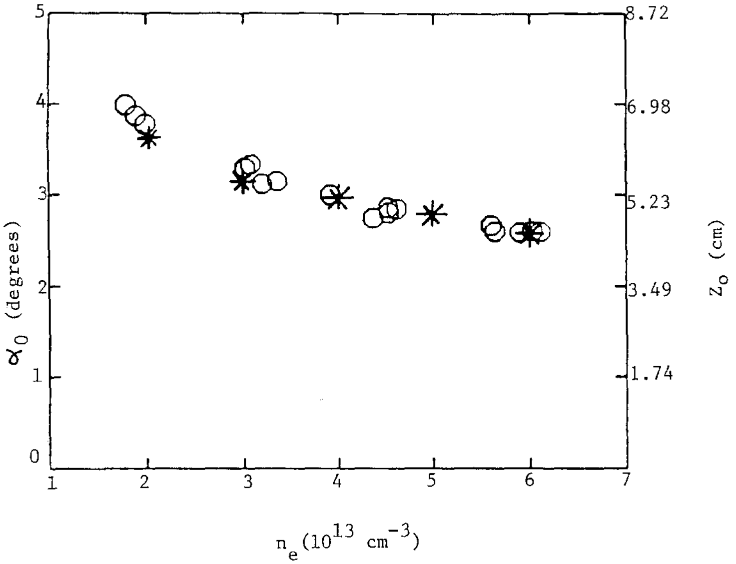

FIG. 4. Toroidal decay length z_0 (expressed as a toroidal exponentiation angle $\alpha_0 = 180z_0/(\pi R_{\text{major}})$ of the source as a function of chord averaged electron density. TEXT major radius is 1 m. The circles are data points from Ref. [20], while the stars are calculations from NUT.

5. SUMMARY

For the neutral transport problem in more than one dimension, we have shown that by separating the small scale variations from the large scale ones and analytically integrating out the small scale features, one can produce an algorithm which is fast and compact enough to be used as part of a larger plasma transport code. The analytical approximation allows one to use a much coarser grid than one would be forced to use without it. Such a code can be useful in cases where the scale lengths of the charged part of the plasma do not vary a lot over different regions. It can also be applied to calculate the source in a reasonably small geometry, such as near a divertor region. It gives the plasma transport simulators a choice which is between the fast one-dimensional codes and the powerful but expensive full three-dimensional simulations.

APPENDIX A

In this appendix, we show the details of the evaluation of the ray integrals $I_i(\mathbf{r}, \omega)$ in Eq. (19). For the plasma-to-plasma case, the integral between two points at distances s_i and s_{i+1} along a ray in the direction ω starting from a given target point $\mathbf{r}$ is given by

$$I_i(\mathbf{r}, \omega) = \int_{s_i}^{s_{i+1}} ds \exp(-f(s))\, \phi(s), \tag{A1}$$

with

$$f(s) = \int_0^s ds'\, a^{\mathrm{tot}}(s, s'), \tag{A2}$$

where $a^{\mathrm{tot}}(s, s')$ is the total inverse mean free path at s' for a neutral born at s with energy equal to $\frac{3}{2}kT$, where T is the local ion temperature. For brevity, we have kept the target point and the ray direction dependence implicit, e.g., we write the source $\chi(\mathbf{r}, s, \omega)$ as $\phi(s)$. Expanding the slowly varying arguments to first order, we get

$$f(s) = f(s_i) + (s - s_i) \left.\frac{df}{ds}\right|_{s_i}, \tag{A3}$$

$$\phi(s) = \phi(s_i) + (s - s_i) \left.\frac{d\phi}{ds}\right|_{s_i}, \tag{A4}$$

which lead to

$$I_i(\mathbf{r}, \omega) = \int_{s_i}^{s_{i+1}} ds \exp[-f(s_i) - (s - s_i)\, f'(s_i)](\phi(s_i) + (s - s_i)\, \phi'(s_i)), \tag{A5}$$

where we denote the derivatives by a prime. These integrals can be performed easily to yield

$$I_i(\mathbf{r}, \omega) = \exp(-f_i)[\alpha_i \phi(s_i) + \beta_i \phi(s_{i+1})], \tag{A6}$$

where

$$f_i = \frac{\delta}{2} \sum_{j=0}^{i-1} [a^{\mathrm{tot}}(s_i, s_{j+1}) + a^{\mathrm{tot}}(s_i, s_j)], \tag{A7}$$

$$\begin{aligned} f_i' = a^{\mathrm{tot}}(s_i, s_i) + \frac{1}{2} \sum_{j=0}^{i-1} [&a^{\mathrm{tot}}(s_{i+1}, s_j) - a^{\mathrm{tot}}(s_i, s_j) \\ &+ a^{\mathrm{tot}}(s_{i+1}, s_{j+1}) - a^{\mathrm{tot}}(s_i, s_{j+1})], \end{aligned} \tag{A8}$$

$$H_i = \frac{1}{f_i'} [1 - \exp(-\delta f_i')], \tag{A9}$$

$$\beta_i = \frac{1}{f_i'} [H_i - \delta \exp(-\delta f_i')], \tag{A10}$$

and

$$\alpha_i = H_i - \beta_i / \delta. \tag{A11}$$

For the plasma-to-wall and wall-to-plasma cases, we get different expressions depending on the wall curvature at the wall point nearest to the plasma point. The surface integral over the wall is broken into integrals over four (or eight) rays along the wall. If we assume a flat wall, the integral over each ray becomes

$$I=\frac{L}{2}\int_0^l dr\,r\,\frac{\exp(-a^{\mathrm{tot}}u)}{u^3}\,\phi(r), \tag{A12}$$

where r, u, and L are the distance shown in Fig. 5a and l is the farthest point on the ray. Again, breaking the integral into pieces and expanding all slowly varying quantities to first order we get the answer as a linear combination of ϕ at points on the ray,

$$I=\frac{L}{2}\sum_{i=0}^{l-1} I_i, \tag{A13}$$

$$I_i=X_i\phi_i+Y_i\phi_{i+1}, \tag{A14}$$

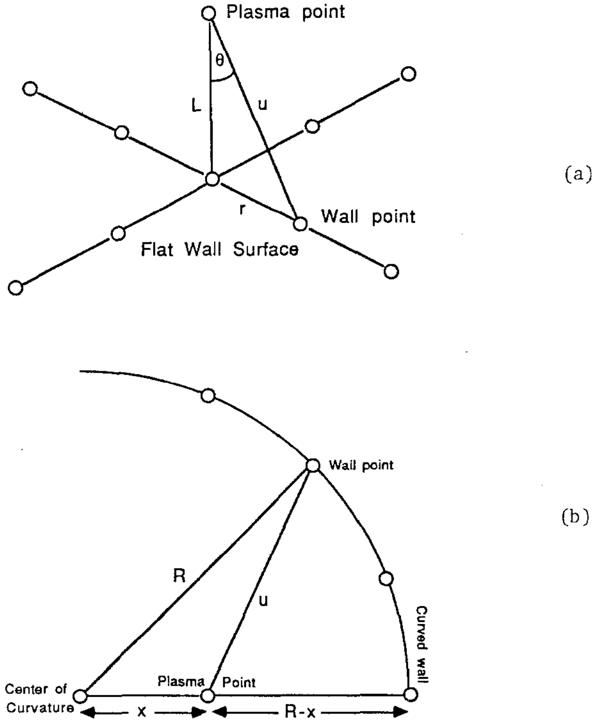

FIG. 5. Geometry for calculation of wall-to-plasma propagators for (a) flat wall and (b) curved wall. The small circles correspond to plasma or wall grid points.

where

$$X_i = \frac{1}{u_{i+1} - u_i}\left(\frac{E_2(\tau)}{u}\bigg|_{i+1}^{i} u_{i+1} - E_1(\tau)|_{i+1}^{i}\right), \tag{A15}$$

$$Y_i = \frac{1}{u_{i+1} - u_i}\left(E_1(\tau)|_{i+1}^{i} - \frac{E_2(\tau)}{u}\bigg|_{i+1}^{i} u_i\right), \tag{A16}$$

and $\tau = a^{\mathrm{tot}} u$. Here the functions E_1 and E_2 are the exponential integral functions

$$E_n(z) = \int_1^\infty dt \, \frac{\exp(-zt)}{t^n}, \tag{A17}$$

for which we use the polynomial approximations given in Ref. [21]. To speed up the program, these can be tabulated and interpolated to required values.

When the wall is not flat, but has a radius of curvature R, we use a similar procedure to obtain

$$I = \frac{1}{4x} \sum_{i=0}^{l-1} I_i, \tag{A18}$$

$$I_i = X_i \phi_i + Y_i \phi_{i+1}, \tag{A19}$$

$$\begin{aligned} X_i = \frac{1}{u_{i+1} - u_i}\bigg[&(R^2 - x^2)\left(\frac{E_2(\tau)}{u}\bigg|_{i+1}^{i} u_{i+1} - E_1(\tau)|_{i+1}^{i}\right) \\ &+ \lambda(\exp(-\tau)|_{i+1}^{i} u_{i+1} - (u+\lambda)\exp(-\tau)|_{i+1}^{i})\bigg], \end{aligned} \tag{A20}$$

$$\begin{aligned} Y_i = \frac{1}{u_{i+1} - u_i}\bigg[&(R^2 - x^2)\left(E_1(\tau)|_{i+1}^{i} - \frac{E_2(\tau)}{u}\bigg|_{i+1}^{i} u_i\right) \\ &- \lambda(\exp(-\tau)|_{i+1}^{i} u_i - (u+\lambda)\exp(-\tau)|_{i+1}^{i})\bigg], \end{aligned} \tag{A21}$$

where x and u are the distances shown in Fig. 5b and $\lambda = 1/a^{\mathrm{tot}}$. Note that for very large R this expression reduces to the flat wall case. However, when R is comparable to the mean free path, the curved wall leads to much larger neutral penetration than the flat one.

In the above, instead of doing the s integral first, we could have done the ω integral first by breaking up the plasma volume around the target point into cubic shells. Since the volume of each shell is proportional to s^2, where s is the shell size, the singular $1/s^2$ factor in the denominator in G again cancels. We could then sum over the shells to get the total integral. In this step, we could make use of the fact that the integrals over the shells decrease like $\exp(-s)$, since the plasma does not vary significantly over a grid length. Hence, instead of using a trapezoidal approximation to calculate the sum over shells (which typically gives an overestimate), we would use an exponential approximation where the integral between two successive shells would be given by $(f_1 - f_2)/(\ln(f_1) - \ln(f_2))$. However, the resulting expression is not linear in ϕ, and so cannot be put into the matrix form of Eq. (15). We therefore do not integrate over ω first.

ACKNOWLEDGMENTS

The author thanks Dr. J. C. Wiley, Dr. D. W. Ross, Dr. William L. Rowan, and Dr. S. Tamor for helpful discussions. This work was supported by DOE Grant DEFG-05-88ER53266.

REFERENCES

1. A. D. Sakharov, *Plasma Phys. Probl. Controlled Thermonucl. React.* **1**, 3 (1961).
2. S. Rehker and H. Wobig, *Plasma Phys.* **15**, 1083 (1973).
3. J. Connor, *Plasma Phys.* **19**, 853 (1977).
4. K. Burrel, *Phys. Fluids* **21**, 2202 (1978).
5. D. F. Duchs, *Bull. Amer. Phys. Soc.* **15**, 1488 (1970).
6. D. F. Duchs, D. E. Post, and P. H. Rutherford, *Nucl. Fusion* **17**, 565 (1977).
7. K. Audenarde, G. A. Emmert, and M. J. Gordiner, *J. Comput. Phys.* **34**, 268 (1980).
8. J. G. Gilligan, *Nucl. Fusion* **18**, 63 (1978).
9. S. Tamor, *J. Comput. Phys.* **40**, 104 (1981).
10. J. T. Hogan, *J. Nucl. Mat.* **111**, 413 (1982).
11. J. H. H. M. Potters and W. J. Goedheer, *Nucl. Fusion* **25**, 779 (1985).
12. M. H. Hughes and D. Post, *J. Comput, Phys.* **28**, 43 (1978).
13. D. B. Heifetz *et al.*, *J. Comput. Phys.* **46**, 309 (1982).
14. D. B. Heifetz and D. Post, *Comput. Phys. Commun.* **29**, 287 (1983).
15. E. Cupini *et al.*, *J. Comput. Phys.* **52**, 122 (1983).
16. S. Saito *et al.*, *Nucl. Technol./Fusion* **4**, 498 (1983).
17. M. Tendler and D. Heifetz, *Fusion Technol.* **11**, 289 (1987).
18. G. M. McCracken and P. E. Stott, *Nucl. Fusion* **19**, 889 (1979).
19. K. W. Gentle, *Nucl. Technol/Fusion* **1**, 479 (1981).
20. W. L. Rowan *et al.*, *J. Nucl. Mat.* **145**, 562 (1987).
21. M. Abramowitz and I. A. Stegun, "*Handbook of Mathematical Functions*" (Dover, New York, 1964), pp. 228.